ARTICLE

Correlating Structure and Properties of Super-concentrated Electrolyte Solutions: ^{17}O NMR and Electrochemical Characterization

Irene Ruggeri,[a]1 Andrea La Monaca,[a]2 Francesca De Giorgio,[a] Francesca Soavi,[a] Catia Arbizzani,*[a] Vittorio Berbenni,[b] Chiara Ferrara,[c] Piercarlo Mustarelli*[c]

Abstract

Super-concentrated electrolyte solutions are of increasing interest for safer and more powerful lithium and post-lithium batteries. The combination of ^{7}Li and ^{17}O (at natural abundance) nuclear magnetic resonance (NMR) and electrochemical characterization is here proposed as an effective approach to investigate the Li^+ solvation structures and properties of electrolytes featuring tetraethylene glycol dimethyl ether (TEGDME) and lithium-bis(trifluoromethane sulfonyl) imide (LiTFSI). Five different formulations from salt-in-solvent to solvent-in-salt with LiTFSI at different concentrations (0.1m, 0.5m, 2m, 4m, 5m) are investigated. The NMR results, also supported by physico-chemical characterizations such as thermal gravimetric analyses, differential scanning calorimetry, specific conductivity and viscosity, give information about the association of Li^+ ions with anion and solvent molecules, so allowing a deeper knowledge on the relationships among structure and functional properties of super-concentrated solutions.

Introduction

The worldwide increase of energy demand has focused a renewed interest toward the use of lithium metal as anode in rechargeable batteries featuring the non-intercalation and low-cost sulfur and oxygen cathode materials.[1]

Li/S and Li/O_2 systems are very attractive for their practical specific energy of ca. 500 mWh g^{-1}, significantly higher than that of lithium-ion batteries that typically deliver up to 250 mWh g^{-1}.[2-5] However, the problems affecting Li metal anode and S and O_2 cathodes are far from being solved, considering that both systems suffer from poor reversibility. The electrochemical Li deposition involves the growth of microstructures, such as fibers and/or dendrites that potentially cross the separator and cause short circuits with related safety issues.[6-9]

Therefore, the choice of a suitable electrolyte for rechargeable batteries with lithium metal anode is crucial because it affects the composition and the properties of the electrode/electrolyte interphase, known as solid electrolyte interphase (SEI). Several efforts have been devoting to understand the reason of an irregular deposition of Li during the charge process and to find strategies to obtain a homogeneous plating. Electrolyte additives able to create a selective inorganic/organic protective layer on Li or the use of novel electrolytes were proposed to stabilize the surface with a tailored SEI.[10-12]

In order to deeply investigate the processes occurring in the novel electrochemical energy storage systems based on lithium metal anode, the combination of electrochemical techniques with bulk and advanced spectroscopic ones is mandatory. In this context, nuclear magnetic resonance (NMR) spectroscopy plays a key role to understand the processes taking place in a battery.[13-16] NMR exploits the magnetic properties of atomic nuclei to find out information on the chemical environment in molecules and solids, as well as on its changes over time. This last task is fulfilled by measuring the relaxation times of chemical species, namely T_1 and T_2. The former is related to the relaxation time of excited nuclear states on the direction of the applied magnetic field (spin-lattice relaxation), whereas the latter is related to the relaxation on the transverse direction (spin-spin relaxation).

Thanks to the relevant technological progresses that made high-magnetic field spectrometers and probes with improved sensitivity available, today it is possible to perform ^{17}O NMR also on solid and viscous samples at natural abundance (0.038%) without the need of isotopic enrichment. This expanded dramatically the capability of the technique, as the lone pairs of the oxygen atoms, available in both solvents and in the anion, directly coordinate Li^+ cations. However, significant problems still hold, chiefly because ^{17}O is a quadrupolar nucleus (nuclear spin I = 5/2) that gives broad and complex spectra under solid or semi-solid conditions. Bogle et al.[17] for the first time performed natural abundance ^{17}O NMR measurements in carbonate-based electrolytes, i.e. ethylene carbonate (EC) and dimethylcarbonate (DMC). Peng et al.[18] characterized a series of glyme-based electrolytes with different length, tetraethylene glycol dimethyl ether (TEGDME) included, featuring lithium-

[a] Dr. I. Ruggeri[1], A. La Monaca[2], Dr. F. De Giorgio, Dr. F. Soavi, Prof. C. Arbizzani
Dept. of Chemistry "Giacomo Ciamician"
Alma Mater Studiorum - University of Bologna
via F. Selmi 2, 40126 Bologna, Italy
E-mail: catia.arbizzani@unibo.it
[b] Prof. V. Berbenni
Dept. of Chemistry and INSTM
University of Pavia
viale T. Taramelli 12, 27100 Pavia, Italy
[c] Dr. C. Ferrara, Prof. P. Mustarelli
Dept. of Materials Science
University of Milano-Bicocca
via R. Cozzi 55, 20125 Milano, Italy
E-mail: piercarlo.mustarelli@unimib.it

[1]Present address: ZSW - Zentrum für Sonnenenergie- und Wasserstoff-Forschung Baden-Württemberg, Helmholtzstraße 8, 89081 Ulm, Germany

[2]Present address:Centre d'excellence en électrification des transports et stockage d'énergie, Hydro-Québec, 1806 Boulevard Lionel-Boulet, Varennes, Québec J3X 1S1, Canada. Centre Énergie, Matériaux et Télécommunications, Institut National de la Recherche Scientifique, 1650 Boulevard Lionel-Boulet, Varennes, Quebec, Canada J3X 1S2.

Supporting information for this article is given via a link at the end of the document.

trifluoromethanesulfonate ($LiCF_3SO_3$) and lithium-bis(trifluoromethane sulfonyl) imide (LiTFSI) as salts. This study suggested a favored coordination of Li^+ with the glyme oxygen atoms. Deng et al.[19] collected natural abundance ^{17}O spectra of LiTFSI in EC, propylene carbonate (PC) and ethyl methyl carbonate (EMC), and noticed that ion pairs association occurred in highly concentrated LiTFSI/EC/EMC/PC solutions. Specifically, Li^+ ion is coordinated by four oxygen atoms by the organic solvent molecules and the anion to form a first solvation shell. At high concentrations of LiTFSI, the preferred structures are $(LiTFSI)_2(PC)_4$ for LiTFSI in PC, and $(LiTFSI)_2(EMC)_3$ for LiTFSI in EMC. Li^+ diffusion assisted by two solvent molecules was reported by Hayamizu et al.[20] in their seminal NMR work on relatively concentrated TEDGME-based electrolyte, featuring 1.12 m and 2.25 m LiTFSI.

Wan et al.[21] performed natural abundance ^{17}O NMR and ^6Li to investigate the solvation structures of Li^+ at various concentrations of lithium-bis(fluorosulfonyl)imide (LiFSI) in 2-dimethoxyethane (DME) solutions. The authors noticed that the ^{17}O chemical shifts changed with the Li^+ concentration, addressing the different solvation structures in the investigated electrolytes. Indeed, in dilute concentrations (<1 M), the majority of cation complexes are Li^+-$(DME)_3$ with a small amount of LiFSI-$(DME)_2$. At Li concentration higher than 2 M, the LiFSI-(DME) complex is the most diffuse form, while the $Li^+(FSI^-)_2$-DME is formed for the 4 M electrolyte.

Super-concentrated and solvent-in-salt (SIS) solutions, i.e. solution with nearly equal molar amount of salt and solvent, have positive impact on cycling and safety performance of Li/S batteries thanks to a beneficial effect on the anode SEI, by preventing the dendrite formation.[22]

The increase of the electrolyte concentration is a multi-effective strategy to improve the performance of high energy batteries featuring Li metal anode. SISs with a low anion transference number can minimize the polarization and the electric field, delaying the dendrite formation at the metal surface. Indeed, during the deposition of Li^+ on Li metal, the free space created by the anion depletion is minimized, inhibiting irregular dendrite nucleation.[23] The decreased number of free molecules of solvent in SIS suppresses also the continuous parasitic reactions between the electrolyte and the anode, thus positively affecting the SEI stability.

In this paper electrolytes based on TEGDME and LiTFSI at various concentrations from salt-in-solvent to solvent-in-salt are investigated by multinuclear NMR, including ^7Li and ^{17}O at natural abundance. The NMR results are here presented and discussed along with the electrochemical characterization carried out with the aim to investigate the feasibility of using the proposed electrolyte systems in lithium metal batteries.

Results and Discussion

Figure 1 shows the ^{17}O NMR spectra of the 0.1m, 0.5m, 2m, 4m, 5m and Table 1 reports the full details of peaks best-fits. The spectrum of the sample 0.1m shows two peaks at -3 and -23 ppm (right panel), which are attributed to middle and terminal oxygens of the TEGDME chain, respectively.[18] The shape of both the peaks is Lorentzian, which means that the quadrupolar interaction is fully averaged at room temperature. The spectrum of 0.5m is characterized by a partial merging of the TEGDME peaks, with a clear asymmetry upfield. This is likely due to the onset of electric quadrupole coupling between the ^{17}O nucleus and the local electric field gradient (EFG), which is no longer fully averaged by Brownian motion due to the increased viscosity of the solution, i.e. 7.1 cP against 3.5 cP of the 0.1m solution (Table S1). As a matter of fact, the simple Lorentzian fit of Figure 1 is not fully satisfying from this point of view. On the other hand, also the attempt to fit

this part of the spectrum with two quadrupolar sites (see Figure S1) does not fully account for the upfield tail. Better results could be obtained by fitting the peaks in terms of a Czjzek distribution of quadrupolar coupling constants, C_Q, which gives values in the range 0.5-4 MHz depending on the site (see Figure S1).[24, 25] We recall here that the Czjzek model provides a joint probability distribution $f_C(V_{zz}, \eta_Q)$ of the principal value V_{zz} of the EFG tensor and of the quadrupolar asymmetry parameter η_Q. The spectrum of 2m in Figure 1 suggests that the increased viscosity of the solution gives origin to a well-defined 2nd order quadrupolar feature in the range 0-400 ppm, due to all the oxygen nuclei of TEGDME, with $C_Q \cong 9.5$ MHz and quadrupolar asymmetry parameter, $\eta_Q \cong 0$. The occurrence of a 2nd order spectral feature calls for a partial reduction of the motional averaging effect, similar to that obtained under Magic Angle Spinning, which operates a C_3 symmetry averaging, in comparison with the C_∞ one made by Brownian motion.

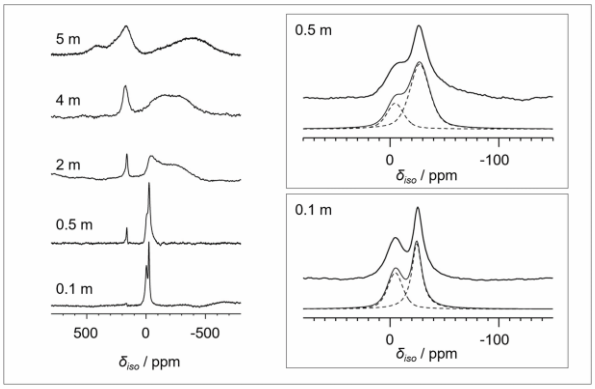

Figure 1 The left panel shows the ^{17}O NMR spectra of the 0.1m, 0.5m, 2m, 4m and 5m electrolytes. The right panel shows the region of TEGDME peaks for the 0.1m and 0.5m electrolytes. In both cases, the upper spectrum represents the experimental one, whereas the lower one is its best-fit in terms of two Lorentzian curves reported with their sum.

Table 1 ^{17}O and ^{7}Li NMR parameters of the samples 0.1m, 0.5m, 2m, 4m, 5m, and comparison with the data taken from the literature for pure TEGDME and 1m LITFSI-TEGDME. c.s. = chemical shift; FWHH = Full Width at Half Height; T_1 = spin-lattice relaxation time; T_2 = spin-spin relaxation time.

Sample	TEGDME -(CH_2-CH_2-O-CH_2-CH_2)-				TEGDME -(CH_2-O-CH_3)				$TFSI^-$				
	c.s. (ppm)	FWHH (Hz)	^{17}O T_1 (μs)	^{17}O T_2 (μs)	c.s. (ppm)	FWHH (Hz)	^{17}O T_1 (μs)	^{17}O T_2 (μs)	c.s. (ppm)	FWHH (Hz)	%	^{17}O T_1 (μs)	^{7}Li T_1 (ms)
TEGDME[a]	-2.5	456	n.a.	n.a.	-23.2	250	n.a.	n.a.	-	-	-	-	-
0.1	-3.0	850	290	280	-23.4	550	507	500	162.2	~500	-	-	598
0.5	-3.7	850	145	145	-23.5	1140[b]	342	290	162.1 178.2	508 813	77 23	720	644
1[a]	-3.9	928	n.a.	n.a.	-23.6	651	n.a.	n.a.	162.0	298	100	n.a.	-
2	[c]		~70	~70	[c]		~70	~70	161.1 178.5	630 734	89 11	~70	459
4	-	-	-	-	-	-	-	-	160.4 178.2	1200 805	90 10	-	380
5	-	-	-	-	-	-	-	-	[d]		-	-	598

[a] From Ref. (20) at 333K. [b] Value overestimated due to the spectral asymmetry (see the text below). [c] Single quadrupolar site: $C_Q \cong 9.5$ MHz, $\eta_Q \cong 0$.
[d] Single quadrupolar site: $C_Q \cong 11$ MHz, $\eta_Q \cong 0$

For the more concentrated 4m and 5m solutions, the quadrupolar interaction gets even stronger and the spectral features due to the TEGMDE oxygen atoms are smeared out on a wider frequency window.

According to the chemical shifts of the TEGDME peaks collected in Table 1 and to the data reported in Ref. 18, the peaks are shifted upfield for the increasing salt concentration, which was attributed to the interaction with the Li^+ ions.[18] The absolute chemical shift variation is larger for chain oxygens than for terminal ones. This means that in these solutions the Li^+ ions are

coordinated by a ring structure to form the $[Li(TEGDME)_1]^+$ cation complex, where oxygens in the glyme chain are more strictly connected to Li^+ respect to low concentrated solutions. The results are in agreement with early ^{13}C NMR studies on TEDGME-$LiClO_4$.[26] Coordination of LiTFSI up to five oxygens was reported by Mao et al.[27] on the PEO-LiTFSI system.

Coming to the region near 160 ppm, the spectrum of 0.1m shows a small spectral feature, which is attributed to the oxygen atoms of $TFSI^-$.[18] This feature increases, as expected, by increasing the salt concentration up to 4m. Figure 2 displays in this spectral region, for 0.5m, 2m and 4m, the presence of two peaks at about 160 and 178 ppm, whose chemical shifts, line-widths and relative percentages are reported in Table 1.

Since the ion pairs interaction leads to the decrease of the electronic charge on the $TFSI^-$ oxygen atoms,[18] we can attribute the upfield peak (at ~160 ppm) to associated salt molecules, and the peak at 178 ppm to the dissociated moieties.

From the best fits of Figure 2, we observe that the association degree increases from 0.77 to 0.90 passing from 0.5m to 4m solutions.

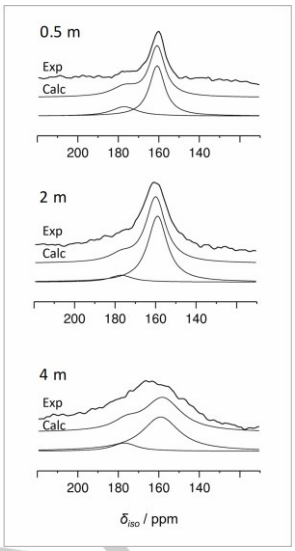

Figure 2 Experimental and calculated ^{17}O NMR spectra of LiTFSI salt for samples 0.5m, 2m, 4m.

Finally, in sample 5m (see Figure 1) we observe the onset of a quadrupolar feature similar to that found in the TEGDME region for 2m, but for the reverse intensity of the maxima, which can be attributed to a distribution of the quadrupolar coupling constants.[29] The best fit gives $C_Q \cong 11$ MHz, $\eta_Q \cong 0$.

The ^7Li NMR spectra display small (~0.2 ppm) shift upfield from 0.1m to 5m electrolytes, accompanied by a line-width increase from ~100 Hz to ~150 Hz, which are due to progressive ions association and increase of viscosity, respectively (see Figure S2). It was not possible to discriminate the contributions of separated ions and ion pairs because of the small chemical shift range of ^7Li.

Finally, it is interesting to consider the dynamic properties of the solutions as revealed by ^{17}O relaxation times. Although it was difficult to measure both T_1 and T_2 for TEGDME because of the low signal-to-noise ratio, the data reported in Table 1 demonstrate that the two relaxation times are practically equal in all cases, as expected in the liquid state.[30] In this regime, the quadrupolar-driven relaxation rates are given by the Equation (1):[30]

$$\left(\frac{1}{T_1}\right)_Q = \left(\frac{1}{T_2}\right)_Q = \frac{3}{10}\pi^2 \frac{2I+1}{I^2(2I-1)} C_Q^2 \left(1+\frac{\eta_Q^2}{3}\right)\tau_c \qquad (1)$$

where τ_c is the correlation time and I is the spin number (I = 5/2 for ^{17}O). If we interpolate to the composition 2m the correlation times reported for TEGDME by Hayamizu et al.,[20] we obtain τ_c = 1.85×10^{-10} s, which inserted in the Equation (1) gives $C_Q \cong 9.13$ MHz, in excellent agreement with the value obtained by fitting the spectrum of Figure 1. ^7Li T_1 data are also reported in Table 1. Such data are in agreement with Hayamizu et al.[20] that obtained values of ~500 ms and ~400 ms for 1.22 m and 2.25 m, respectively. We stress here that the ^{17}O NMR quadrupolar parameters, C_Q and η_Q, are here reported for the first time in case of such TEGDME-LiTFSI concentrated solutions.

Table 2 reports the ratios of the oxygen atoms of TEGDME and the Li^+ ions, the glass transition temperature (T_g) and the melting

temperature (T_m) according to the DSC measurements (Figure S3).

Table 2 Thermal properties of TEGDME and of 0.1m, 0.5m, 2m, 4m and 5m LiTFSI solutions: T_g = glass transition temperature; T_m = melting temperature; ΔH_m = melting enthalpy.

Sample	n=[O_{TEGDME}]/[Li]	T_g (°C)	T_m (°C)	ΔH_m (Jg^{-1})
TEGDME[a]	-	-	-30[a]	-
0.1m	224.92	-65.02	-30.44	151.1
0.5m	45.00	-64.35	-33.05	88.5
2m	11.25	-	-31.40	1.1
4m	5.62	-	-30.62	0.09
5m	4.50	-56.20	-31.77	2.40

[a] From Ref. (20) at 333K.

As expected, by increasing the salt concentration in the investigated electrolytes, the mobility of the ions decreases, presumably due to the ionic-couple formation and to the increase of the solution viscosity (Table S1). The ionic conductivity of 0.5m and 5m at 20°C are 1.76 and 0.73 mS cm^{-1} and the viscosity 7.1 and 550 cP, respectively. Furthermore, the thermal stability increases with the salt concentration, being related to the intermolecular interaction among particles. Indeed, according to the TGA data reported in Figure S3a, TEGDME is stable up to 100°C, while the degradation of 5m starts at 300°C.

The DSC thermograms and the related data are reported in Figure S3b and Table 2, respectively. There is a general decrease of the melting enthalpy, ΔH_m, of TEGDME at about 30°C as the salt concentration increases. This is probably due to the progressive complexation of Li^+ ions by TEGDME molecules, as also suggested by NMR (see Table 1).[20] Glass transition features can be observed below -50/-65 °C for 0.1m, 0.5m and 5m. Interestingly, in 2m and 4m electrolytes there is not any visible glass transition and the ΔH_m of TEGDME reaches the lowest values of 1.1 and 0.09 J g^{-1}, respectively.

The absence of glass transition calls for the “strong” nature (in the sense of Angell’s fragility concept) of these glass-forming liquids.[31] In contrast, the glass transition is visible again in the sample 5m. This counterintuitive result can be rationalized by a non-linear behavior of the activity coefficient, which can increase towards the unity at elevated concentrations. More detailed studies, which are out of the scope of the present paper, are needed to address this point. The overall NMR and thermal results of the LiTFSI-TEGDME electrolytes suggest that the Li^+ ions in concentrated solutions (4m and 5m) are mostly associated with their $TFSI^-$ anions and, at the same time, are coordinated by one or, at most, two TEGDME molecules. Hence, by increasing the concentration of Li salt, the TEGDME solvent is more involved to coordinate the Li^+ cation than in less concentrated solutions. Indeed, while in the 0.5m there are 45 oxygen atoms of TEGDME corresponding to ca. 9 molecules per each Li^+, in the 5m there are only 4.5 oxygen atoms of TEGDME, corresponding to just one molecule allowed to form the $[Li\ (TEGDME)_1]^+$ cation complex (see Table 2). In order to better investigate how the structure and properties of such electrolyte systems can affect the electrochemical response, voltammetric and galvanostatic measurements were performed. The NMR findings and the electrochemical performance have been thus correlated to prove the feasibility of combining them in the characterization of Li metal batteries. Figure 3a and Figure 3b show the first and fifth cyclic voltammogram (CV) at 10 mV s^{-1} of Pt electrode in 0.5m, 2m, 4m and 5m. The CVs were carried out in the range -0.45 V and 2.20 V vs. Li^+/Li. Figures 3c-3f show the single CVs of the selected electrolytes. The cathodic peak corresponds to the Li deposition on Pt electrode, while the anodic peak at ca. 0.25 V vs. Li^+/Li is related to the bulk stripping process of the alkali metal. In all the investigated electrolytes, the anodic peaks at potentials higher than 0.50 V vs. Li^+/Li can be attributed to the oxidation of intermetallic Li-Pt alloys formed during the cathodic scan, as already reported by Wibowo et al.[32] The peak current is related to

the diffusion coefficient (D) and concentration (C) of the redox species at the interphase. Hence, it is expected that the increase of the Li concentration affects the peak current of the CVs. Although the Li source increases with the salt concentration, the current related to the bulk process of Li deposition/stripping decreases in the investigated electrolytes. Indeed, I_{red} and I_{ox} of 5m and 0.5m are -0.15 mA and 0.07 mA and -0.70 mA and 0.50 mA, respectively. Such findings can be attributed to the decrease of the D_{Li+} with the increase of Li salt concentration, since this parameter is affected by the viscosity.[33] This is indirectly confirmed by the reduction of ^{7}Li T_1 by a factor of two passing from 0.5m to 5m, which again points towards a stronger ion interaction with the lattice. It is worth noting that 2m and 4m show similar DSC thermograms (see Table 2 and Figure S3b) and similar peak currents, although such electrolytes have different viscosities, i.e. ca. 30 cP and ca. 90 cP, respectively (see Table S1). In 2m and 4m electrolytes, the two contributions of the increased C and the decreased D are likely balanced. According to the ^{17}O NMR results reported in Table 2, the number of TEGDME molecules that coordinate the Li^+ cation decreases with the increase of Li^+ concentration, whereas the $TFSI^-$ anion amount close to Li^+ increases with the concentration. Beside the D_{Li+} reduction, the decrease of I_{red} with the Li concentration may be also related to the lower TEGDME amount that is electrochemically reduced to form an electrode/electrolyte interphase on Pt. Figure S4 displays the SEM images of the Li electrode used as counter electrode during the Li stripping/deposition in 0.5m and 4m electrolytes. The SEM analysis evinces that the composition of the SEI formed in both electrolytes is different. As per EDX analysis (Table S2), while the SEI layer formed in 0.5m is thick and mainly composed of organic molecules, the SEI formed in 4m is thinner and mainly composed of inorganic molecules, due to the $TFSI^-$ decomposition (Table S2).

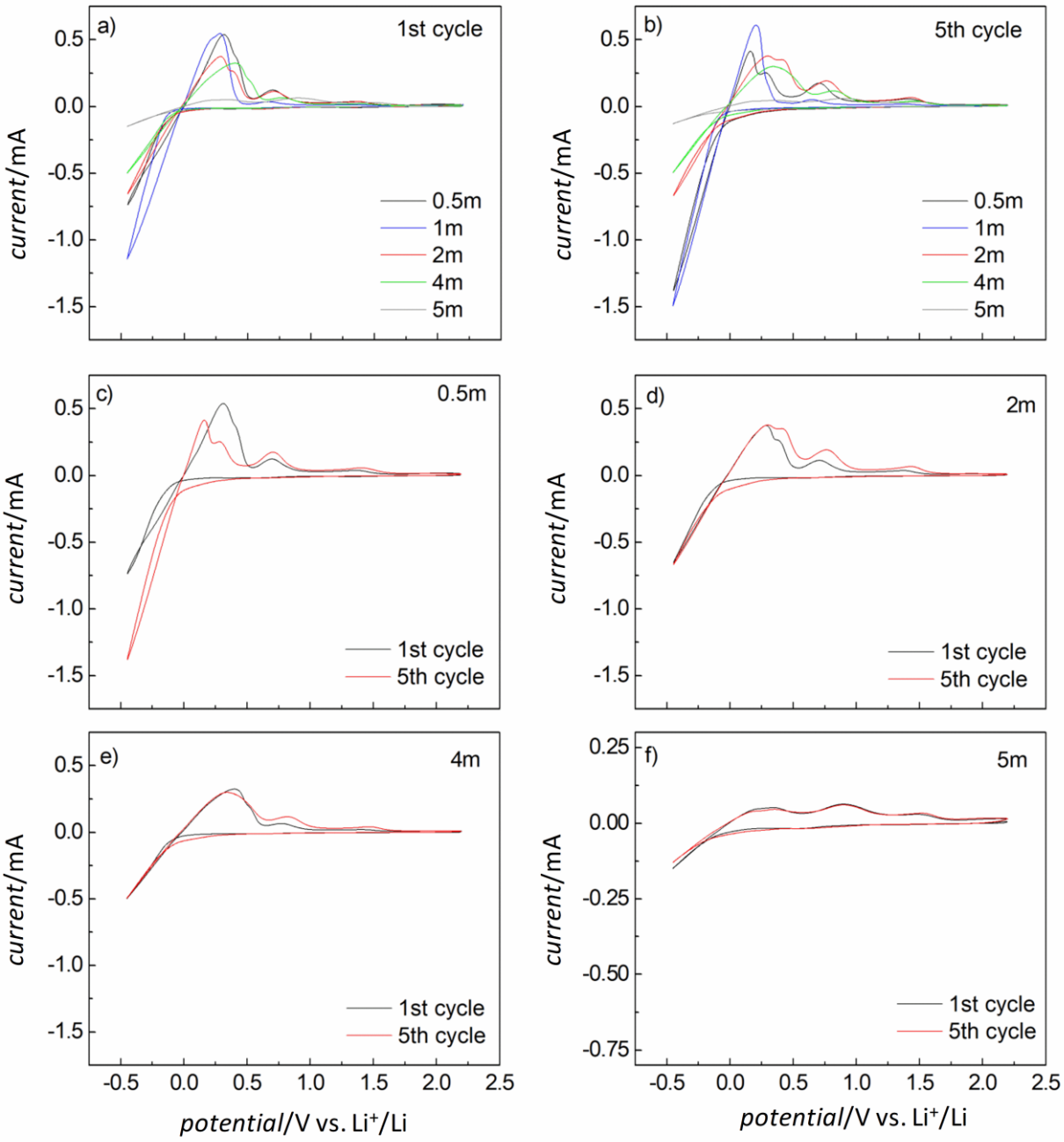

Figure 3 CVs (1st and 5th cycle) at 10 mV s^{-1} of Pt electrode tested in 0.5m, 2m, 4m and 5m electrolytes.

Table 3 reports the onset potential (V_{red}) of Li^+ reduction, the reduction (Q_{red}) and oxidation (Q_{ox}) charge and the coulombic efficiency ($\eta = Q_{ox}/Q_{red}$) of the first and fifth CVs shown in Figure 3. The V_{red} of the first and fifth CVs are shifted towards more positive potentials as the ionic concentration increases, probably due to the lower energy amount that the free Li^+ cations need to deposit in metallic and/or alloy by increasing salt concentration.

Table 3 Onset potential (V_{red}) of Li^+ reduction, the reduction (Q_{red}) and oxidation (Q_{ox}) charge and the coulombic efficiency ($\eta = Q_{ox}/Q_{red}$) of the first and fifth CVs shown in Figure 3.

Electrolyte	1st CV				5th CV			
	V_{red} (V)	Q_{red} (mC)	Q_{ox} (mC)	η	V_{red} (V)	Q_{red} (mC)	$Q_{ox.}$ (mC)	η
0.5m	-0.130	-35.5	21.5	0.61	-0.083	-62.6	18.6	0.30
2m	-0.113	-28.6	17.2	0.60	-0.043	-32.8	24.2	0.74
4m	-0.070	-22.3	15.7	0.71	-0.063	-23.3	18.9	0.81
5m	-0.045	-8.6	7.1	0.83	0.001	-8.2	7.0	0.86

The Q_{red} values decrease with the increase of ionic concentration and considerably increase in 0.5m electrolyte from the 1st to the 5th cycle. On the contrary, Q_{red} slightly increases in 2m and 4m and sharply decreases in 5m. The η values increase with the ionic concentration. The coulombic efficiency and the reduction charge also increase with the cycle number in 2m and 4m electrolyte, probably due to the decrease of side reactions related to the SEI formation as the cycling proceeds. A massive Li deposition at low Li concentration is involved in a considerable SEI formation. Indeed, by limiting the cathodic scan at – 0.25 V vs. Li^+/Li (see Figure S3), in 0.5m electrolyte the η values are similar to those obtained in super-concentrated solutions during the CVs carried out with a cut-off of – 0.45 V vs. Li^+/Li (see Figure S3 and Table S3).

These results suggest that the bulk process of Li plating/stripping becomes more reversible upon cycling. The η values lower than 100% testify that the amount of Li plated during the reduction does not totally oxidized back to Li^+ during the anodic scan. This may explain why the Li deposition, especially at low concentration, occurs at more positive potentials. Indeed, the Li nucleation step has skipped, resulting in an increase of Q_{red} and I_{red}. However, the increase of I_{red} upon cycling in 0.5m can be also due to a net Li^+ concentration increase because of chemical reactions occurring during the formation of SEI that releases Li^+ at the interphase.[34]

The anodic peaks at 0.15 V vs. Li^+/Li of the fifth CV of Figure 3c and of Figure S5, Table S3 (first and fifth) are related to the Li stripping in 0.5m electrolyte. In 5m, the first anodic and broader peak occurs at more positive potential (ca. 0.25 V vs. Li^+/Li), suggesting that the Li stripping is related to the oxidation of Li involved in the formation of the alloy with Pt and is probably hindered by the high viscosity of the electrolyte.

All these findings suggest that in 2m and 4m electrolytes, which are similar from a thermodynamic point of view as they do not show any glass transition and have very low melting enthalpy for TEGDME, the Li deposition/stripping process is mainly characterized by a slight passivation of the Li metal. This is confirmed by the NMR results (Table 2), which show that the number of TEGDME molecules that coordinate Li^+ is lower in 2m and 4m than in 0.5m.

Galvanostatic tests on Li/Li symmetrical cells at 0.1 mA cm^{-2} and 0.2 mA cm^{-2} in 0.5m, 2m, 4m and 5m solutions were performed, and the cell voltage profiles are shown in Figure 4. While the charge/discharge processes in 2m and 4m electrolytes show a similar behavior at both current densities, the processes in 5m seems more hindered, likely because of a slower Li^+ diffusion in agreement with the viscosity data. The spikes in the voltage profiles of the cell with 0.5m electrolyte at 0.2 mA cm^{-2} are presumably due to the formation of an irregular SEI layer.

Even though the 2m and the 4m electrolytes feature different viscosity, ionic conductivity and number of TEGDME molecules per Li^+ (ca. 2 vs. 1 in 2m and 4m, respectively), they have similar overvoltage values of ca. 200 mV at low current densities (0.1 and 0.2 mA cm^{-2}) as shown in Figure 5. The Figure shows the charge/discharge cycles performed at currents densities from 0.1 to 0.6 mA cm^{-2} by the same cells reported in Figure 4 featuring 2m

and 4m electrolytes. In the cell with 2m (Figure 5a), Li dendrite formation clearly occurs, probably starting from the cycles at 0.3 mA cm^{-2}, as evinced by the rapid decrease of the overvoltage. In contrast, in case of the 4m solution no significative overvoltage reduction due to Li dendrite formation is observed, even at higher current densities (Figure 5b). Figure 5c shows the comparison of the cell voltage profiles at 0.4 mA cm^{-2}. The use of 4m solution can be thus well suited in the low-middle current range.

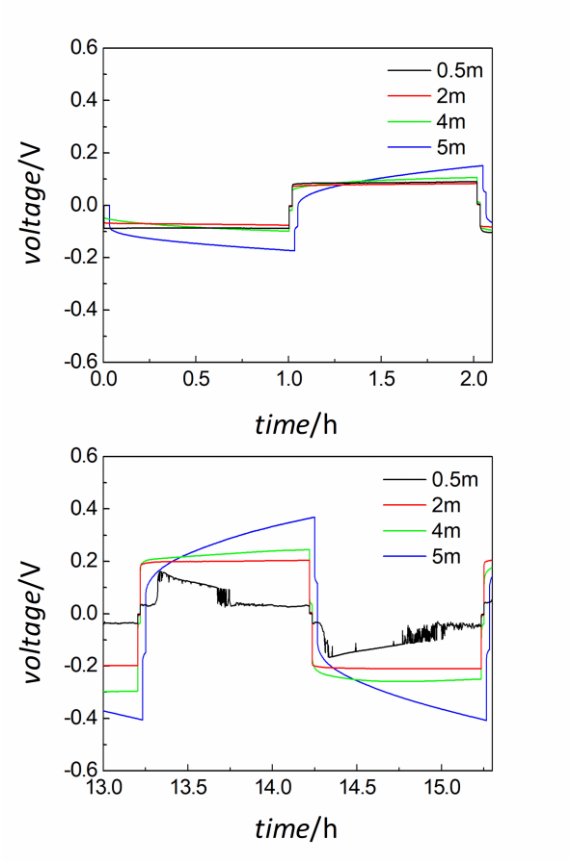

Figure 4 Cell voltage profiles during 1h discharge - 1h charge cycles at 0.1 mA cm^{-2} (a) and 0.2 mA cm^{-2} (b) carried out in T-shaped Li//Li cells (0.785 cm^2) with 0.5m, 2m, 4m and 5m.

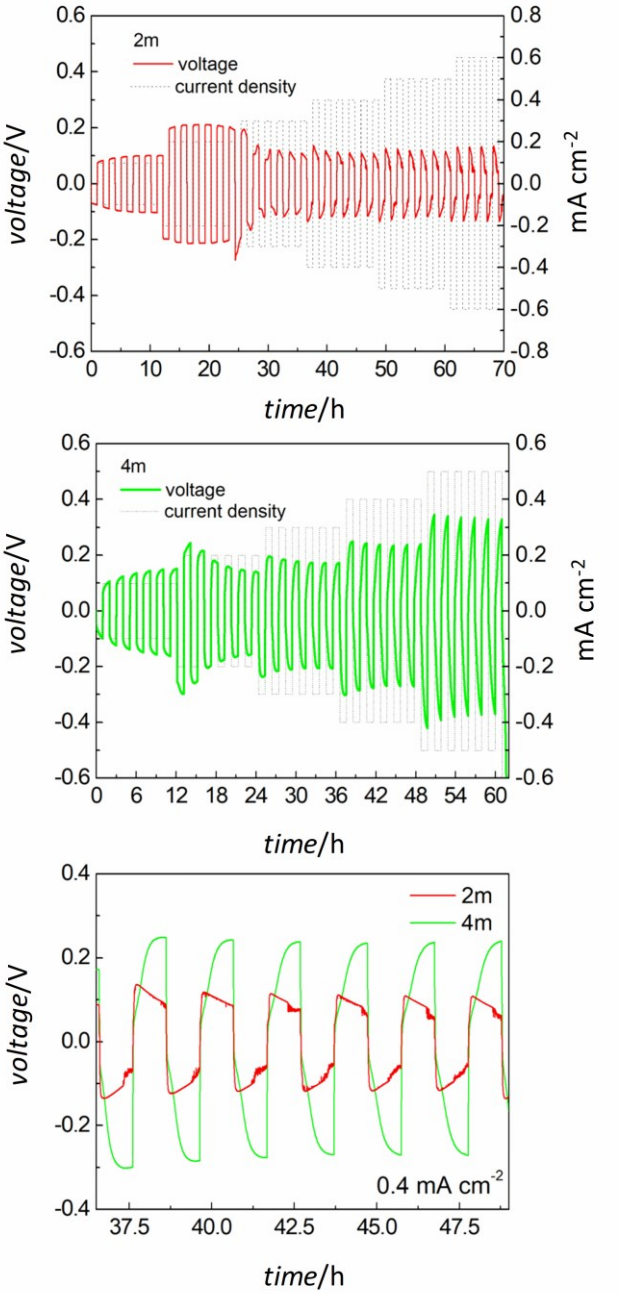

Figure 5 Voltage profiles of 1h discharge - 1h charge cycles performed in 3-electrode mode in T-shaped Li//Li cells (0.785 cm^2) with 2m and 4m electrolytes at 0.1, 0.2, 0.3, 0.4, 0.5 and 0.6 mA cm^{-2}. Cell voltage and current density profiles of 2m (a), 4m (b) and comparison of cell voltage at 0.4 mA cm^{-2} (c). The potential cut-offs are – 2.00 V / 2.00 V vs. Li^+/Li.

Conclusions

The combination of nuclear magnetic resonance (NMR) including ^{7}Li and ^{17}O at natural abundance, and electrochemical characterization allowed us to perform a deep investigation of solvation structures of Li^{+} in electrolyte based on TEGDME and LiTFSI at different formulations, i.e. from salt-in-solvent to solvent-in-salt (0.1m, 0.5m, 2m, 4m, 5m). The NMR results and thermal analyses demonstrate that Li^{+} ions in concentrated solutions (4m and 5m) are chiefly associated with their $TFSI^{-}$ anions and are coordinated by one or maximum two TEGDME molecules. The NMR results also demonstrate that in 2m and 4m electrolytes the number of TEGDME molecules that coordinate Li^{+} is much lower than in 0.5m. Such findings are confirmed by the electrochemical results, which demonstrated that in 2m and 4m electrolytes the Li deposition/stripping process is mainly characterized by a slight passivation of the lithium metal surface. At these electrolyte concentrations, SEI is mainly formed of inorganic molecules due to $TFSI^{-}$ decomposition. The super-concentrated solution based on TEGDME and 4m LiTFSI is well suited for the use in lithium metal batteries operating in the low-middle current range.

Experimental Section

Lithium-bis(trifluoromethane sulfonyl) imide (LiTFSI, ≥99%, Aldrich) was dried under vacuum at 120°C for 48 h and stored in argon-filled dry box (LabMaster SP, MBraun, O_2 and H_2O < 0.1 ppm). Tetraethylene glycol dimethyl ether (TEGDME, 99%, Aldrich, H_2O=20 ppm) was used without further purification. The LiTFSI-TEGDME solutions were prepared and stored in dry box. Li metal (300 µm thickness) was supplied by Chemetall and stored in the dry box. The molality of the investigated solutions was 0.1 (only for calorimetric and NMR analyses), 0.5, 2, 4 and 5, corresponding to a solvent-to-salt molar ratio of 9, 2.3, 1.1 and 0.9, respectively. The solutions were labelled 0.1m, 0.5m, 1m, 2m, 4m, 5m.

^{17}O NMR spectra were collected with a 400 MHz Bruker Avance III spectrometer (9.4 T magnet) equipped with a wideline probe (^{17}O Larmor frequency = 54.243 MHz). The samples were sealed in Ar-filled glove box (H_2O, O_2 < 1 ppm) and measured immediately. Single-pulse experiments were performed at room temperature for each composition with 128 k – 1024 k scans, delay time of 0.1 s, pulse length of 20 µs with 100 kHz spectral window. Signals were referred to liquid H_2O (0 ppm). No signal filtering was performed. ^{7}Li data were acquired at room temperature on a 4 mm MAS probe under static conditions. Indeed, MAS experiments could allow a better understanding of the NMR. Unfortunately, although relatively viscous, our samples are still liquid enough not to be spin into our standard 7 mm MAS probe (zirconia rotors and kel-f caps). We tried to perform these MAS experiments, but the rotation was slow and uneven. In order to spin such viscous materials, specific MAS systems are needed.[35, 36] The NMR signals have been referred to LiCl aq (0 ppm). Single pulse experiments have been acquired with 516 scans, pulse length of 3.5 µs and delay time of 5 s. Spin-lattice relaxation times (T_1) were obtained at room temperature for both ^{17}O and ^{7}Li by using the standard Inversion Recovery (180°-τ-90°) sequence.

Thermal analyses included thermal gravimetric analysis (TGA) and differential scanning calorimetry (DSC). TGA was performed with a TA Instruments Q50 apparatus, by heating each sample from room temperature to 500°C at 10 °C/min under argon flow. DSC measurements were carried out using a DSC Q2000 (TA Instruments). For each composition, ~6-7 mg was weighed inside the glove-box and sealed into Al pans, to perform the thermal treatment from -80 °C to 150 °C at a heating rate of 10°C/min. The enthalpies associated to melting and crystallization processes were obtained by the integration of the area of the DSC peaks with the TA Universal Analysis Software.

Cyclic voltammetry of different electrolytes (4 mL) was performed in dry box at room temperature (RT) using a glass cell with Pt disk (4 mm diameter) as working electrode and Li as counter and reference electrode. The electrochemical characterization of Li was also performed by galvanostatic deposition/stripping cycles on symmetric Li//Li T-shaped Teflon® cells (Bola, Bolhender GmbH) at 30 °C in three-electrode mode with a Li reference electrode. The electrochemical tests were carried out by PerkinElmer VMP and Biologic VSP multichannel potentiostats/galvanostats.

Scanning electron microscopy (SEM) images and energy-dispersive X-ray spectroscopy (EDX) were carried out with a High-Resolution Field Emission Electron Microscope Zeiss Merlin Compact VP Oxford EDX detector with 50 mm² chip area.

Acknowledgements

The authors thank for financial support MIUR-DAAD Joint Mobility Program “Interface properties of electrode materials" and Dr. Alexander Dinter (Landshut Hochschule) for assistance in SEM analyses.

Keywords: solvent in salt solutions (SIS) • glyme • ^{17}O NMR • ^{7}Li NMR

[1] D. Lin, Y. Liu, Y. Cui, *Nature Nanotechnology* **2017**, *12*, 194–206.

[2] B. Scrosati, J. Garche, W. Tillmetz, **2015,** *Advances in Battery Technologies for Electric Vehicles;* Woodhead Publishing, Elsevier Ltd.: Cambridge, UK.

[3] R. Van Noorden, *Nature* **2014**, *507*, 26-28.

[4] H. Zhang, X. Li, H. Zhang, **2017,** *Li–S and Li–O_2 Batteries with High Specific Energy: Research and Development*; Springer Nature: Singapore.

[5] P. G. Bruce, S. A. Freunberger, L. J. Hardwick, J. M. Tarascon, *Nature Materials* **2012**, *11*, 19–29.

[6] Y. Guo, H. Li, T. Zhai, *Adv. Mater.* **2017**, *29*, 1700007.

[7] W. Xu, J. Wang, F. Ding, X. Chen, E. Nasybulin, Y. Zhang, Y. G. Zhang, *Energy Environ. Sci.* **2014**, *7*, 513–537.

[8] Z. Li, J. Huan, B. Y. Liaw, V. Metzler, J. Zhang, *J. Power Sources* **2014**, *254*, 168–182.

[9] K. J. Harry, D. T. Hallinan, D. Y. Dilworth, Parkinson, A. A. MacDowell, P. Nitash, N. P. Balsara, *Nat. Mater.* **2014**, *13*, 69-73.

[10] Q. Wang, C. Yang, J. Yang, K. Wu, L. Qi, H. Tang, Z. Zhang, W. Liu, H. Zhou, *Energy Storage Materials* **2018**, *15*, 249–256.

[11] N. D. Trinh, D. Lepage, D. Aymé-Perrot, A. Badia, M. Dollé, D. Rochefort, *Angew. Chem. Int. Ed.* **2018**, *57*, 5072–5075.

[12] X. B. Cheng, R. Zhang, C. Z. Zhao, F. Wei, J. G. Zhang, Q. Zhang, *Adv. Sci.* **2016**, *3*, 1500213.

[13] O. Pecher, J. Carretero-Gonzalez, K. J. Griffith, C. P. Grey, *Chem. Mater.* **2017**, *29*, 213−242.

[14] Hu, J. Z.; Jaegers, N. R.; Hu, M. Y.; Mueller, K. T. In Situ and Ex Situ NMR for Battery Research. *J. Phys.: Condens. Matter* **2018**, *30*, 463001.

[15] H. J. Chang, N. M. Trease, A. J. Ilott, D. Zeng, L. S. Du, A. Jerschow, C. P. Grey, *J. Phys. Chem. C* **2015**, *119*, 16443−16451.

[16] F. Blanc, M. Leskes, C. P. Grey, *Acc. Chem. Res.* **2013**, *46*, 1952-1963.

[17] X. Bogle, R. Vazquez, S. Greenbaum, A. von Wald Cresce, K. Xu, *J. Phys. Chem. Lett.* **2013**, *4*, 1664−1668.

[18] J. Peng, L. Carbone, M. Gobet, J. Hassoun, M. Devanye, S. Greenbaum, *Electrochim. Acta* **2016**, *213*, 606–612.

[19] X. Deng, M. Y. Hu, X. Wei, W. Wang, Z. Chen, J. Liu, J. Z. Hu, *J. Power Sources* **2015**, *285*, 146-155.

[20] I. Hayamizu, K. Sugimoto, E. Akiba, Y. Aihara, T. Bando, W. S. Price, *J. Phys. Chem. B* **2002**, *106*, 547-554.

[21] C. Wan, M. Y. Hu, O. Borodin, J. Qian, Z. Qin, J. G. Zhang, J. Z. Hu, *J. Power Sources* **2016**, *307*, 231-243.

[22] L. Suo, Y. S. Hu, H. Li, M. Armand, L. Chen, *Nat. Commun.* **2013**, *4*, 1481.

[23] M. D. Tikekar, S. Choudhury, Z. Tu, L. A. Archer, *Nat. Energy* **2016**, *1*, 16114.

[24] P. Florian, N. Sadiki, D. Massiot, J. P. Coutures, *J. Phys. Chem. B* **2007**, *111*, 9747−9757.

[25] C. Ferrara, C. Tealdi, P. Mustarelli, M. Hoelzel, A. J. Pell, G. Pintacuda, *J. Phys. Chem C* **2014**, *118*, 15036-15043.

[26] D. Fish, J. Smid, *Electrochim. Acta* **1992**, *37*,2043-2049.

[27] G. Mao, M. L. Saboungi, D. L. Price, M. B. Armand W. S. Howells, *Phys. Rev. Lett.* **2000**, *84*, 5536-5539.

[28] L. Carbone, J. Peng, M. Agostini, M. Gobet, M. Devany, B. Scrosati, S. Greenbaum, J. Hassoun, *ChemElectroChem* **2017**, *4*, 209 – 215.

[29] P. Mustarelli, R. Riccardi, S. Scotti, M. Villa, *Phys. Chem. Glasses* **1991**, *32*, 129-131.

[30] A. Abragam, *The Principles of Nuclear Magnetism*, **1961,** Oxford University Press: London.

[31] M. Tatsumisago, B. L. Halfpap, J. L. Green, S. M. Lindsay, C. A. Angell, *Phys. Rev. Lett.* **1990**, 64, 1549-1552.

[32] R. Wibowo, S. E. Ward Jones, R. G. Compton, *J. Phys. Chem. B* **2009,** *113*, 12293–12298.

[33] F. Messaggi, I. Ruggeri, D. Genovese, N. Zaccheroni, C. Arbizzani, F. Soavi, *Electrochim. Acta* **2017**, *245*, 296–302.

[34] A. Basile, A. F. Hollenkamp, A. I. Bhatt, A. P. O'Mullane, *Electrochem. Commun.* **2013**, *27*, 69–72.

[35] E.D. Walter, L. Qi, A. Chamas, H.S. Mehta, J.A. Sears, S.L. Scott, D.W. Hoyt, *Journal of Physical Chemistry C* **2018**, *122*, 8209-8215.

[36] N.R. Jaegers, M.Y. Hu, D.W. Hoyt, Y. Wang, J.Z. Hu, *Modern Magnetic Resonance* **2018**, 1073-1091.

Entry for the Table of Contents

Layout 1:

ARTICLE

The combination of nuclear magnetic resonance (NMR) including ^{7}Li and ^{17}O at natural abundance and electrochemical characterization is a powerful and effective approach to perform a deep investigation of solvation structures of Li^{+} in electrolyte based on TEGDME and LiTFSI, from salt-in-solvent to solvent-in-salt.

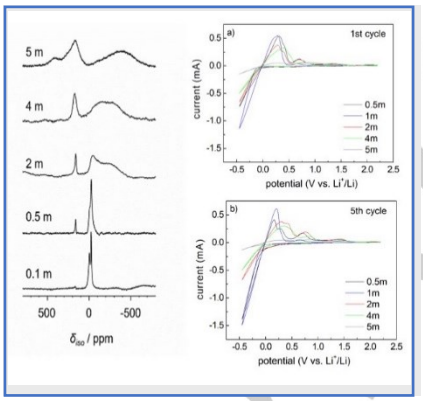

Irene Ruggeri, Andrea La Monaca, Francesca De Giorgio, Francesca Soavi, Catia Arbizzani, Vittorio Berbenni, Chiara Ferrara, Piercarlo Mustarelli**

Page No. – Page No.

Correlating Structure and Properties of Super-concentrated Electrolyte Solutions: ^{17}O NMR and Electrochemical Characterization